AMERICAN SOCIETY FOR MICROBIOLOGY | Journal of Virology®

VIRUS-CELL INTERACTIONS

Endoplasmic Reticulum-Associated Degradation Controls Virus Protein Homeostasis, Which Is Required for Flavivirus Propagation

Keisuke Tabata,[a,b] Masashi Arakawa,[c] Kotaro Ishida,[c] Makiko Kobayashi,[c] Atsuki Nara,[d] Takehiro Sugimoto,[e] Tetsuya Okada,[e] Kazutoshi Mori,[e] Eiji Morita[c]

[a]Laboratory of Intracellular Membrane Dynamics, Graduate School of Frontier Biosciences Osaka University, Osaka, Japan
[b]Department of Genetics, Graduate School of Medicine, Osaka University, Osaka, Japan
[c]Department of Biochemistry and Molecular Biology, Faculty of Agriculture and Life Science, Hirosaki University, Aomori, Japan
[d]Nagahama Institute of Bio-Science and Technology, Nagahama, Japan
[e]Department of Biophysics, Graduate School of Science, Kyoto University, Kyoto, Japan

Keisuke Tabata, Masashi Arakawa, and Kotaro Ishida contributed equally to this work. Author order was determined on the basis of seniority.

ABSTRACT Many positive-stranded RNA viruses encode polyproteins from which viral proteins are generated by processing the polyproteins. This system produces an equal amount of each viral protein, though the required amounts for each protein are not the same. In this study, we found the extra membrane-anchored nonstructural (NS) proteins of Japanese encephalitis virus and dengue virus are rapidly and selectively degraded by the endoplasmic reticulum-associated degradation (ERAD) pathway. Our gene targeting study revealed that ERAD involving Derlin2 and SEL1L, but not Derlin1, is required for the viral genome replication. Derlin2 is predominantly localized in the convoluted membrane (CM) of the viral replication organelle, and viral NS proteins are degraded in the CM. Hence, these results suggest that viral protein homeostasis is regulated by Derlin2-mediated ERAD in the CM, and this process is critical for the propagation of these viruses.

IMPORTANCE The results of this study reveal the cellular ERAD system controls the amount of each viral protein in virus-infected cells and that this "viral protein homeostasis" is critical for viral propagation. Furthermore, we clarified that the "convoluted membrane (CM)," which was previously considered a structure with unknown function, serves as a kind of waste dump where viral protein degradation occurs. We also found that the Derlin2/SEL1L/HRD1-specific pathway is involved in this process, whereas the Derlin1-mediated pathway is not. This novel ERAD-mediated fine-tuning system for the stoichiometries of polyprotein-derived viral proteins may represent a common feature among polyprotein-encoding viruses.

KEYWORDS *Flavivirus*, endoplasmic reticulum-associated degradation, Derlin2, valosin-containing protein, convoluted membrane, ERAD, VCP

Viruses belonging to the genus *Flavivirus* encode a single polypeptide, from which viral proteins are generated by cellular and viral proteases. This system has the advantage of encoding more information in a small genome while allowing for the synthesis of each adjacent viral protein required for the formation of the viral replicase complex with a limited copy number of viral genomes (1). However, this system retains considerable disadvantage in controlling the amount of each viral protein. For instance, although the need for viral structural proteins, required for generation of progeny virions, is much higher than the need for nonstructural (NS) proteins, which

Citation Tabata K, Arakawa M, Ishida K, Kobayashi M, Nara A, Sugimoto T, Okada T, Mori K, Morita E. 2021. Endoplasmic reticulum-associated degradation controls virus protein homeostasis, which is required for flavivirus propagation. J Virol 95:e02234-20. https://doi.org/10.1128/JVI.02234-20.

Editor J.-H. James Ou, University of Southern California

Address correspondence to Eiji Morita, moritae@hirosaki-u.ac.jp.

Received 19 November 2020
Accepted 29 April 2021
Accepted manuscript posted online 12 May 2021
Published 12 July 2021

function as biochemical catalysts, yet the same amount of structural and NS proteins are generated from a single polypeptide. Thus, viruses must discard extra NS proteins that are synthesized concomitantly with structural proteins. This homeostasis of viral protein levels is considered essential for viral propagation, though the mechanisms of this control system have not yet been clarified.

The *Flaviviridae* is a family of positive, single-stranded RNA viruses, including dengue virus (DENV), Japanese encephalitis virus (JEV), West Nile virus, yellow fever virus, and Zika virus. These viruses are transmitted by infected arthropods and cause severe human diseases. Translation of viral RNA leads to the production of a single polyprotein (~3,400 amino acids), which is cleaved into three structural proteins (capsid, prM, and E) and seven nonstructural proteins (NS1, NS2A, NS2B, NS3, NS4A, NS4B, and NS5) by viral and host cellular proteases (2). The structural proteins form the virus particles, which are ultimately released from the cells, whereas NS proteins are involved in RNA genome replication by forming a specific compartment called the replication organelle, comprising two different areas known as vesicle packets (VPs) and convoluted membrane (CM) (3). VPs contain a few dozen small vesicles packed in the outer membrane and represent the location of the viral genome synthesis. Meanwhile, CM form a reticulovesicular network of membranes and is considered to function as a place for storage, or the processing of membrane-anchored viral proteins (4).

Endoplasmic reticulum (ER)-associated degradation (ERAD) is a highly conserved quality control system that recognizes misfolded ER proteins and transports them to the cytoplasm for proteasomal degradation (5, 6). During this process, misfolded substrates are ubiquitylated on the cytosolic side by ER-associated ubiquitin ligases such as HRD1 or gp78. Ubiquitylated substrates are then extracted from the membrane by valosin-containing protein (VCP)/p97, the conserved ATPase associated with diverse cellular activities (AAA-ATPase), and delivered to the 26S proteasome for degradation. HRD1 forms a complex with homologues of the yeast Hrd1p complex members, including SEL1L, OS-9, Derlin1/2/3, and HERP, whereas gp78 forms a complex with UbxD8, UBAC2, UBE2G2, and Derlin1 (7). These complexes are further categorized based on their composition, each of which recognizes substrates based on their misfolded regions (8, 9). Previously, several genetic screening studies identified ERAD components, including Derlin2, SEL1L, and HRD1, as important for flavivirus replication (10, 11). However, the molecular mechanisms underlying the roles of these components in viral genome replication remain largely unknown.

In this study, we aimed to determine if membrane-anchored viral NS proteins are selectively degraded by the Derlin2-mediated ERAD pathway at the CM. This degradation of NS proteins is required to maintain viral protein homeostasis, which is critical for viral genome replication in host cells.

RESULTS

A subset of JEV and DENV nonstructural proteins is selectively and rapidly degraded in infected cells. To investigate changes in the level of each viral protein within JEV-infected cells, we performed cycloheximide (CHX) chase followed by Western blotting, using specific antibodies for all viral proteins, except for NS2A due to the unavailability of antibody (Fig. 1A and B). We identified that the amounts of NS1, NS2B, NS4A and NS4B proteins were rapidly reduced in these cells, compared to those of capsid, E, NS3, and NS5. Among them, the reduction of NS2B, NS4A, and NS4B was significantly impaired by the treatment of MG132, a proteasome inhibitor (Fig. 1C), suggesting that these reductions are caused by proteasomal degradation. Similar results were also observed in DENV-infected cells (Fig. 1D), suggesting that these are common features of JEV- and DENV-infected cells. Moreover, NS2B, NS4A, and NS4B, which are ER membrane-integrated proteins, were found to be ubiquitylated in the cells (Fig. 1E), suggesting their degradation is mediated by the ERAD pathway. However, NS1 is a secreted protein and thus we cannot exclude the possibility that its observed reduction was due to its secretion from cells.

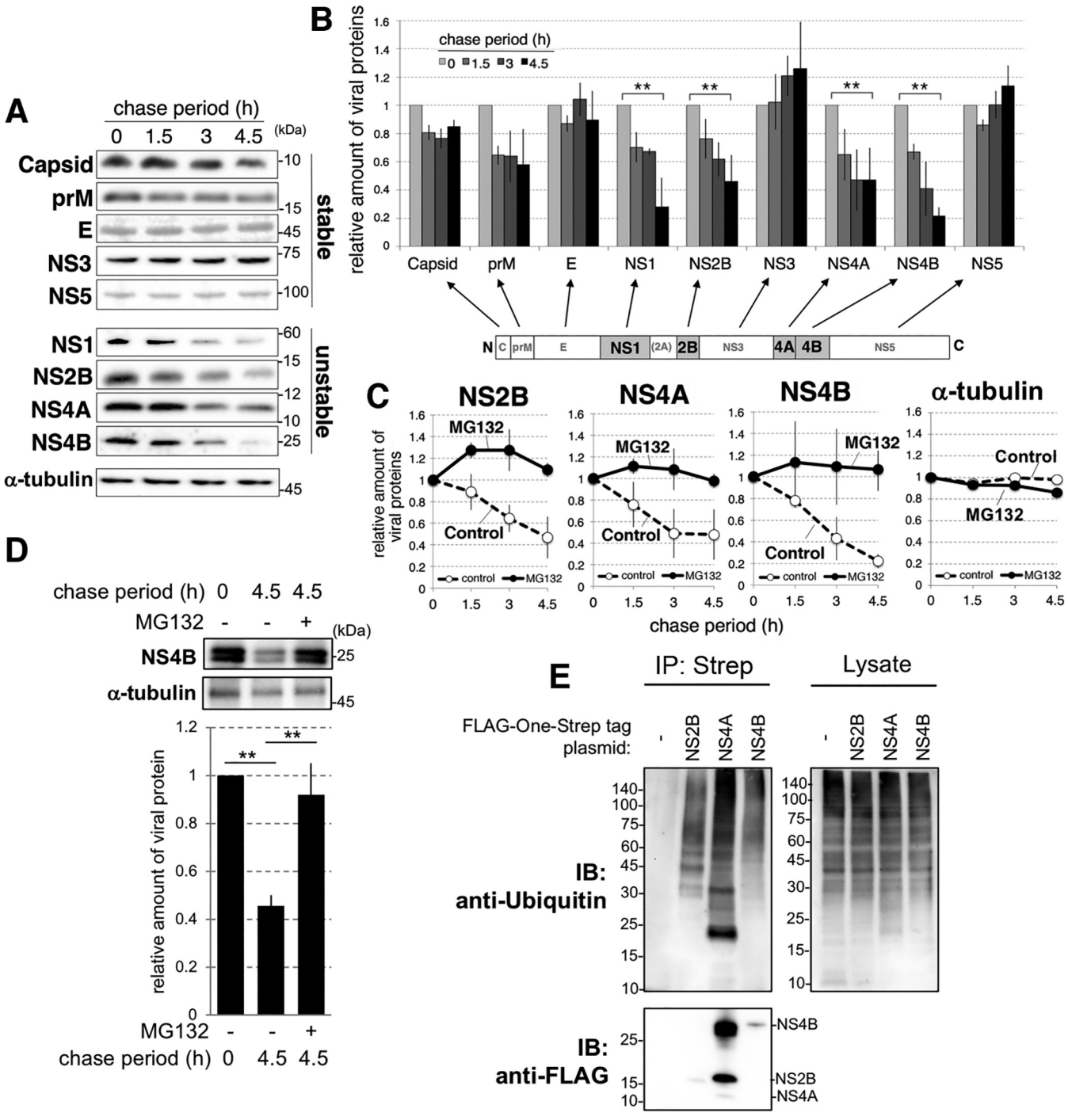

FIG 1 Stability of viral proteins in JEV- or DENV-infected cells. (A) Analysis of each JEV protein degradation by cycloheximide (CHX) chase analysis. HCT116 wild type (WT) cells infected with JEV (MOI = 1) for 48 h were treated with 50 μg/ml CHX and collected at the indicated time points. Cell lysates of infected cells were prepared and analyzed by Western blotting using the indicated antibodies. (B) The relative amount of viral proteins in A was quantified from three independent experiments and normalized to the values for α-tubulin at each point. **, $P < 0.05$, calculated by Student's *t* test. (C) Inhibition of JEV NS2B, NS4A, NS4B, and α-tubulin degradation under proteasome inhibitor treatment. HCT116 WT cells infected with JEV (MOI = 1) for 48 h were treated with 10 μM MG132 2 h before CHX chase analysis as described in A and the relative amount of viral proteins was quantified and normalized to the baseline value at the zero time point. For NS2B, NS4A, and NS4B data, error bars indicate standard deviation. For the α-tubulin data, the value is the average of two independent experiments. (D) Dengue virus NS4B is degraded by the proteasome. HCT116 WT cells infected with DENV (MOI = 1) for 24 h were treated with or without 10 μM MG132 2 h before treatment with 50 μg/ml cycloheximide (CHX) and collected at the indicated time points. Cell lysates of infected cells were prepared and analyzed by Western blotting using the indicated antibodies (upper panel). The relative amount of viral proteins was quantified using the results of three independent experiments and normalized to the baseline values at the zero time point (bottom panel). **, $P < 0.05$, calculated by Student's *t* test. (E) Degradative NS proteins are ubiquitinated. Human 293T cells were transfected with FOS-tagged JEV NS2B, JEV-NS4A, or JEV-NS4B. Expressed proteins were purified with Strep-Tactin Sepharose beads and ubiquitinated proteins in the bound fraction were detected using anti-ubiquitin (top left) or anti-FLAG (bottom) antibodies. Ubiquitinated proteins in the input lysate fraction (Lysate) were also detected (right).

VCP is required for JEV and DENV propagation. To identify cellular factors associated with the degradation process, we performed proteome analysis for the binding factors of NS4B, the NS protein found to be the most significantly degraded. JEV-NS4B and DENV-NS4B, tagged with FLAG One STrEP (FOS), were expressed and affinity-purified from HEK293T cells; copurified cellular proteins were then identified by liquid chromatography-tandem mass spectrometry (LC-MS/MS). We also performed the same experiment using cells transfected with an empty vector and identified cellular proteins bound nonspecifically to the affinity beads. Following elimination of these nonspecific binders, a total of 105 proteins were identified in both JEV-NS4B and DENV-NS4B coprecipitates, with VCP determined to be the most consistent factor in this proteomic screening (Fig. 2A, Table S1 in the supplemental material). Nuclear protein localization protein 4 (NPL4) and ubiquitin recognition factor in ER-associated degradation protein 1 (UFD1), two well-known VCP-associated factors (12), were also identified by this screening process. To confirm the interaction between VCP and JEV NS4B, we carried out pulldown experiments using OSF (One STrEP FLAG)-VCP-expressing cells infected with JEV. As shown in Fig. 2B, JEV NS4B coprecipitated with OSF-VCP. We next investigated the colocalization of VCP with NS4B in JEV-infected cells (Fig. 2C) or cells expressing JEV NS4B (Fig. 2D) and found that VCP colocalized at the puncta with JEV-NS4B. This colocalization was also detected in the cells cotransfected with OSF-VCP and DENV NS4B (Fig. 2E), suggesting that both JEV- and DENV-NS4B interact with VCP complexes.

To validate the role of the VCP complex and ERAD pathway in JEV infection, we assessed the effect of VCP knockdown on viral propagation. Treatments with two different small interfering RNAs (siRNAs) reduced endogenous VCP expression to nearly undetectable levels (Fig. 2F and G) without any cytotoxicity (Fig. 2H), while also significantly reducing the infectious titers of both JEV and DENV (Fig. 2I). Additionally, the viral protein levels (Fig. 2F and G) and intracellular viral RNA levels (Fig. 2J) were significantly decreased. To elucidate the role of VCP in the postentry step, we prepared *in vitro*-transcribed infectious JEV RNA and performed the same knockdown experiments on infectious viral RNA-transfected cells (Fig. 2K). As a result, VCP knockdown significantly impaired JEV propagation even in the viral RNA-transfected cells, indicating that VCP was required for virus replication in the postentry step.

VCP enzymatic activity is vital for virus replication and viral protein degradation. VCP belongs to the AAA-ATPase family of proteins (13). VCP contains two conserved AAA-ATPase domains (D1 and D2) (Fig. 3A), and mutations in these domains impair its ATPase activity. To determine the importance of VCP ATPase activity, we examined whether the point mutations that disrupt the ATPase activity of D1 and/or D2 inhibit VCP function in flavivirus growth by using a siRNA depletion and rescue assay (Fig. 3B). As expected, the inhibition of flaviviral growth by VCP depletion was rescued by overexpressing a wild-type protein. In contrast, the overexpression of VCP with a mutated D1 ATPase domain (E305Q) was not as capable of rescuing viral growth. Meanwhile, VCP mutated at either the C-terminal D2 ATPase domain (E578Q) or both D1 and D2 ATPase domains (E305Q/E578Q) were unable to rescue the defects in viral growth, although all mutant VCPs were expressed normally (Fig. 3B). These results confirm previous results, indicating that ATPase activity, especially the activity of the C-terminal D2 ATPase domain, is critical for VCP function (14).

To further confirm the importance of ATPase activity in viral propagation, we treated cells with specific small compounds, such as DBeQ (15), MDBN (16), and eeyarestatin I (EerI), that inhibit the ATPase activity of VCP (17). These treatments impaired the production of infectious JEV and DENV without exerting potent cytotoxicity (Fig. 3C to F). This inhibitory effect was also observed during viral genome replication in JEV subgenome replicon-transfected cells (Fig. 3G and H). Further, we assessed whether VCP inhibition impairs viral protein degradation. As shown in Fig. 3I, DBeQ treatment of virally infected cells completely inhibited the degradation of NS2B, NS4A, and NS4B in CHX chase experiments. We also observed that the unfolded protein responses (UPRs) were upregulated in virus-infected cells following DBeQ treatment

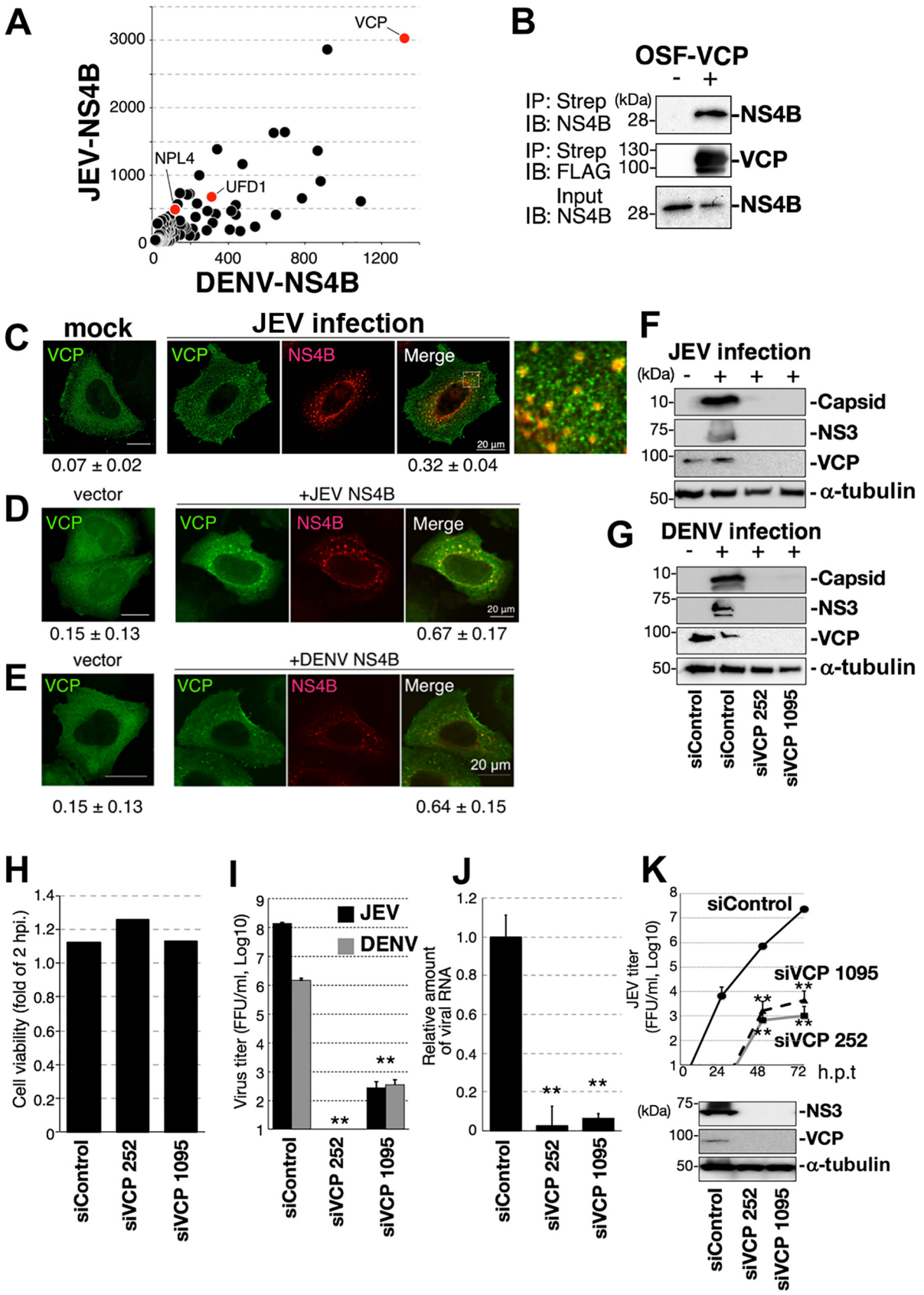

FIG 2 VCP is a host factor required for JEV and DENV propagation. (A) The 2D plot of the Mascot search score of AP-MS analysis using JEV- or DENV-NS4B as bait. A total of 105 proteins identified as common factors binding to both JEV-NS4B and DENV-NS4B in each Mascot

(Continued on next page)

(Fig. 3J). These results indicate that the activities of the ERAD pathway, mediated by VCP, are closely related to viral genome replication in cells.

Derlin2-dependent ERAD pathway is essential for virus genome replication and the degradation of viral NS proteins. To further confirm the involvement of the ERAD pathway in viral genome replication, we tested virus propagation in ERAD component-deficient cells. It was previously proposed that Derlin1 and Derlin2 recognize different substrates in the ERAD pathway (8); therefore, we tested JEV growth in each knockout cell. Interestingly, the deficiency of virus propagation was observed in Derlin2 knockout cells, but not in Derlin1 knockout cells, although the cell growth rate was almost the same (Fig. 4A to C). These results suggest the Derlin2-specific ERAD pathway was involved in viral propagation. Additional knockout of the Derlin3 gene in Derlin2-deficient cells did not show any additive or synergistic inhibitory effect (Fig. 4A and C), while it was previously reported that the expression of Derlin3 is suppressed in HCT116 cells due to DNA methylation (18). These results suggest that Derlin2 deficiency was enough to impair the viral propagation (Fig. 4C). Virus propagation was also impaired in SEL1L knockout cells, and HRD1-depleted cells, supporting the previous observations that both SEL1L and HRD1 function in the same pathway with Derlin2 (8) (Fig. 4C and D). The inhibitory effect of Derlin2 deficiency was also observed in viral genome replication in subgenomic replicon-transfected cells (Fig. 4E). The results suggest the Derlin2/SEL1L/HRD1-mediated ERAD pathway is involved in viral genome replication in the infected cells.

Next, we determined whether the viral growth hindrance via ERAD deficiency was correlated with viral NS protein degradation. NS4B degradation in JEV-infected cells was impaired in Derlin2 deficient cells, but not in wild-type (WT) or Derlin1-deficient cells (Fig. 4F), suggesting that viral growth retardation was caused by defective viral NS protein degradation by the ERAD pathway. To further investigate the relationship between viral protein degradation and viral genome replication, we investigated the effect of excess NS proteins on viral genome replication. Simultaneous expression of NS2B, NS4A, or NS4B with virus subgenomic RNA significantly impaired virus genome replication, whereas overexpression of NS3 or capsid did not show any effects (Fig. 5A). Similar experiments were performed for JEV-infected cells and the results revealed that overexpression of NS2B, but not NS3, impaired JEV propagation (Fig. 5B). These results suggest that excess accumulation of viral NS proteins requiring degradation impairs viral genome replication.

Generally, accumulation of overexpressed proteins can induce UPR and protein kinase RNA-like endoplasmic reticulum kinase (PERK)-mediated translational arrest (19); however, overexpression of NS2B, NS4A, or NS4B did not have this effect (Fig. 5C).

FIG 2 Legend (Continued)
search were plotted on a 2D graph. The horizontal or vertical axis represents a Mascot search score based on DENV-NS4B or JEV-NS4B AP-MS analysis, respectively. VCP and its cofactors are labeled in red. (B) Interaction between JEV-NS4B and VCP was validated using a pulldown assay. Human 293T cells were transfected with pCAG-One-Strep-FLAG (OSF)-VCP and then infected with JEV (MOI = 3.0) for 48 h. The whole-cell lysates (WCL) were prepared and precipitated with Strep-Tactin beads. NS4B in the bead-bound fraction (top) and the WCL (bottom) were visualized by Western blotting using the anti-JEV-NS4B antibody. OSF-VCP in the bead-bound fraction was visualized by anti-FLAG antibody (middle). (C) VCP was colocalized with NS4B. HeLa cells were infected with JEV (MOI = 1) for 24 h and then transfected with pCAG-OSF-VCP. Microscopic images of fixed cells stained with anti-FLAG (green) and anti-JEV NS4B (red) antibodies are presented. (D and E) Colocalization of VCP and JEV NS4B (D) or DENV NS4B (E) in cotransfected cells. HeLa cells were cotransfected with OSF-VCP (green) and JEV-NS4B-Myc (D, red) or DENV-NS4B-Myc (E, red). Microscopic images of fixed cells stained with anti-FLAG (green) and anti-Myc (red) antibodies are presented. Scale bar = 20 μm (C to E). The numbers written under each image indicate the Mander's colocalization coefficient R. (F and G) Effect of VCP knockdown on viral protein expression in JEV- or DENV- infected cells. Human 293A cells were transfected with the indicated siRNAs against control (siControl) or VCP and then infected with JEV (F) for 72 h or DENV (G) for 96 h. Cell lysates were prepared, and the indicated proteins were visualized by Western blotting using the indicated antibodies. (H) VCP knockdown did not affect cell viability. Human 293A cells transfected with the indicated siRNAs were infected with JEV (MOI = 1) for 48 h, and cell viability was assessed using a luminescence-based cell viability assay. Relative luminescence values are shown. The value represents the average of two independent experiments. (I) Effect of VCP knockdown on JEV or DENV propagation. Human 293A cells transfected twice with the indicated siRNAs at a 24 h interval were infected, respectively, with JEV (black bar) for 72 h and DENV (gray bar) for 96 h at an MOI of 0.3. The culture supernatants were collected and the infectious titers were determined by a focus-forming assay. (J) Effects of VCP knockdown on JEV genomic RNA synthesis. Human 293A cells transfected with the indicated siRNAs for 24 h were infected with JEV (MOI = 0.3) for 48 h. The cells were harvested and the relative amount of viral RNA was determined by qRT-PCR and normalized to control siRNA-transfected cells. (K) The effect of VCP knockdown on the virus production from viral genomic RNA-transfected cells. VCP or control siRNA-transfected cells were also transfected with *in vitro*-transcribed full-genomic JEV infectious RNA. The infectious titer for the indicated time points was determined (graph), and the expression level of each protein was validated after 72 h posttransfection (blots).

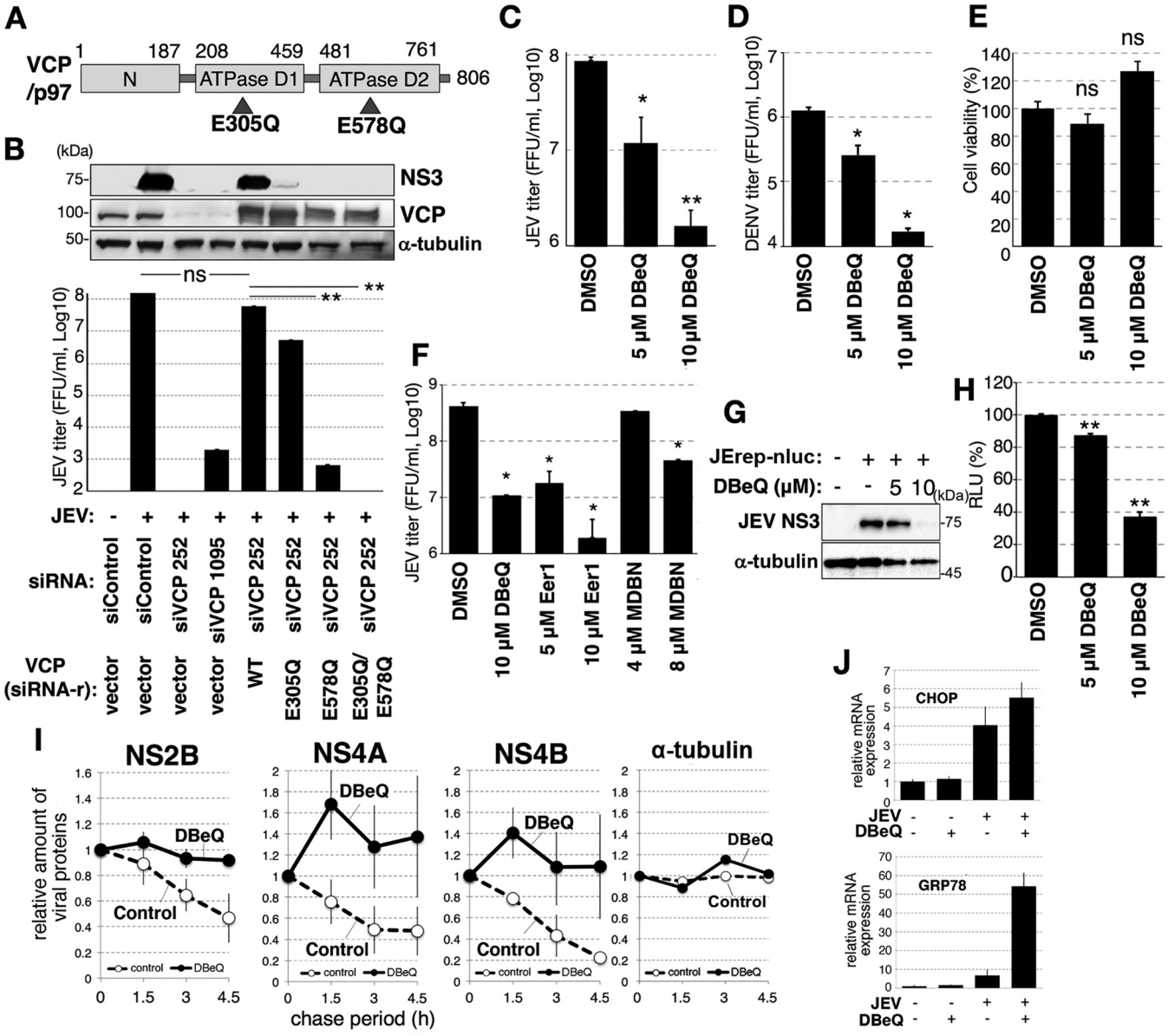

FIG 3 The ATPase activity of VCP is vital for viral propagation and viral protein stability. (A) Domain structure of human VCP, indicating the N-terminal domain (N), two AAA-ATPase domains (D1 and D2), and the ATPase-deficient mutations. (B) Phenotypic rescue of viral propagation by siRNA-resistant VCP constructs. Human 293A cells were cotransfected with pCAG-OSF-VCP or its ATPase-deficient mutant, harboring an siRNA-resistant silent mutation (siRNA-r), and siRNAs against VCP or control. A full time-course of siRNAs and rescue construct transfection are described in our previous paper (20). After two rounds of siRNA transfection and rescue vector cotransfection, the cells were infected with JEV (MOI = 0.3) for 48 h. Cell lysates were prepared, and proteins were detected by Western blotting using the indicated antibodies (blots). Infectious titers of the culture supernatant were determined by a focus-forming assay (graph). **, $P < 0.05$, calculated by Student's *t* test. (C to F) Effects of VCP inhibitors on JEV or DNEV propagation. Human 293A cells were infected with JEV or DENV (MOI = 0.3). After 2 h of virus inoculation, the cells were incubated with VCP inhibitors for 4 h. The culture supernatants of JEV and DENV were collected after 48 hpi or 72 hpi and infectious titers were determined by focus-forming assay. The effects of DBeQ on JEV (C) and DENV (D) propagation were determined. Cell viability at 48 h after JEV infection was determined (E). Effects of DBeQ, Eerl, or MDBN on JEV propagation was determined (F). *, $P < 0.05$, calculated by Student's *t* test. (G and H) Effects of DBeQ on JEV subgenome replication. Human 293T cells were transfected with pCMV-JErep-nluc, followed by treatment with DBeQ for 6 h. The cells were lysed for 24 h after transfection and the protein expression level (G) and luciferase activity (H) were measured. **, $P < 0.05$, calculated by Student's *t* test. (I) Effects of DBeQ on the stability of JEV NS2B, NA4A, NS4B, or α-tubulin. HCT116 wild type (WT) cells infected with JEV (MOI = 1) for 48 h were treated with 10 μM DBeQ at 2 h before treatment with 50 μg/ml CHX and cells were collected at the indicated time points. The relative abundances of JEV NS2B (left), NS4A (middle), and NS4B (right) were quantified by Western blotting and normalized to the baseline value at the zero time point. The error bars for NS2B, NS4A, and NS4B data represent mean standard deviation. For α-tubulin, the data represent the average of two independent experiments. (J) Effects of JEV infection and DBeQ treatment on UPR. HCT116 WT cells infected with JEV (MOI = 1) for 24 h were treated with 10 μM DBeQ for 4 h. The relative levels of GRP78 (bottom) and CHOP (upper) mRNA were determined using qRT-PCR and normalized to actin mRNA levels.

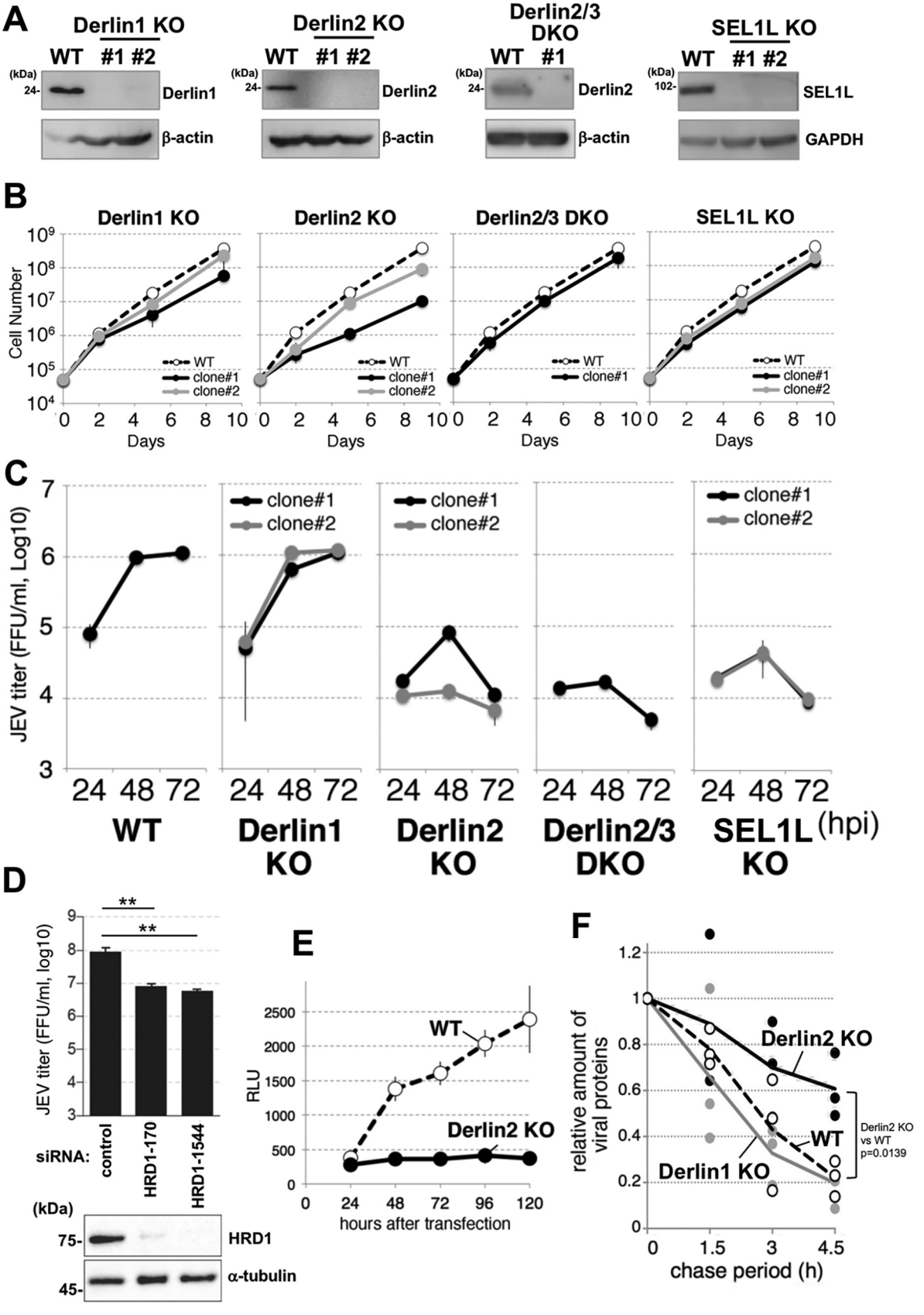

FIG 4 Analysis of JEV propagation on ERAD component-deficient cells. (A) Expression of endogenous Derlin family and SEL1L proteins in each knockout cell. HCT116 cells with knockouts of Derlin1, Derlin2, Derlin2/3, or SEL1L were lysed, and endogenous proteins were

(Continued on next page)

Furthermore, overexpression of NS2B, NS4A, or NS4B impaired viral genome replication in PERK knockout cells (Fig. 5D to F), which could not induce translational arrest in response to treatment with thapsigargin, a Ca^{2+}-ATPase inhibitor (Fig. 5E). These results suggest that the impaired viral genome replication caused by NS protein accumulation is not associated with UPR activation.

CM functions as a site for degradation of viral NS proteins. In specific types of cells, such as Vero and Huh7.5.1 cells, enormous viral replication organelles, which can form clumps up to 5 to 8 μm diameter, are observed after JEV infection (Fig. 6A to D). Our previous correlative light and electron microscopy (CLEM) analysis revealed that the VP and CM in this compartment were distinguishable with specific antibodies for each viral component (20). In this study, we confirmed that double-stranded RNA (dsRNA) and E protein predominantly localize at the VP area, while NS4B and other NS2B proteins localize in the CM area (Fig. 6A to D). Electron microscopy further showed the accumulation of numerus small vesicles at the periphery of these clumps, which likely corresponded to the dsRNA-positive dots (Fig. 6D). Furthermore, a highly electron dense structure with a membrane stack was observed at the center of each clump, corresponding to the CM positive for NS proteins (Fig. 6D). However, CM was observed 24 h postinfection (hpi), while viral protein could be detected after 12 hpi. (Fig. 6E). Furthermore, Derlin2 localized in the CM area detected using CLEM (Fig. 6F). Cumulatively, these results suggest that the CM area may be the site for Derlin2/ERAD-mediated NS protein degradation.

Considering that the levels of NS4B and other viral NS proteins were reduced following CHX treatment (Fig. 1A and B), we performed imaging analysis to investigate whether NS4B was degraded by CHX treatment. After 4.5-h treatment with CHX, JEV-infected Vero cells were stained with antibodies and visualized to assess NS4B and dsRNA localization. The staining pattern of NS4B in the viral replication organelle was altered by CHX treatment (Fig. 6G and H) compared to that in untreated cells (Fig. 6A). Furthermore, the NS4B signal within the center of the clumps, which was not stained with dsRNA antibodies, disappeared in CHX-treated cells (Fig. 6G and H). Meanwhile, these alterations were impaired by treatment with DBeQ or MG132 (Fig. 6G and H), suggesting that NS4B in the CM may be predominantly degraded by the ERAD pathway.

We also assessed the cellular expression of JEV-NS4B. Immuno-electron microscopy analysis showed that NS4B expression alone induced similar clumps in the perinuclear region of virus-infected cells (Fig. 6I). These structures have stacked membranes with NS4B proteins and resemble the CM in JEV-infected cells (Fig. 6I). However, the size of this compartment was reduced by CHX treatment, which in turn was impaired by the addition of DBeQ (Fig. 6J). These altered NS4B levels were also confirmed by Western blotting (Fig. 6K). Cumulatively, these results suggest that NS4B protein may be degraded by the ERAD pathway.

DISCUSSION

In this study, we demonstrated that specific viral NS proteins, namely, NS2A, NS4A, and NS4B (not NS3, NS5, or structural proteins) are degraded by the VCP/Derlin2-mediated

FIG 4 Legend (Continued)
detected using Western blotting. (B) Growth rates of cells with Derlin family and SEL1L knockouts. Total number of Derlin1, Derlin2, Derlin2/3, or SEL1L knockout HCT116 cells at the indicated time points. Two independent knockout cell clones were tested and compared to the parental wild-type (WT) HCT116 cells. (C) Kinetics of JEV growth in ERAD component-deficient cells. HCT116 wild type (WT) cells, as well as Derlin1, Derlin2, Derlin2/3, and SEL1L-knockout cells, were infected with JEV (MOI = 0.3). The culture supernatants of infected cells were collected at the indicated times and the infectious titer was determined by a focus-forming assay. (D) Effect of HRD1 knockdown on JEV propagation. Human 293A cells transfected with HRD1 siRNAs twice with 24 h intervals were infected with JEV for 48 h at an MOI of 0.3. Cells were harvested, and endogenous HRD1 and α-tubulin were detected by Western blotting (bottom). The culture supernatants were harvested, and the infectious titers were determined by a focus-forming assay (upper). **, $P < 0.05$, calculated by Student's *t* test. (E) Comparison of the JEV subgenome replication kinetics between WT and Derlin2-knockout cells. HCT116 WT cells and Derlin2-knockout cells were transfected with pCMV-JErep-nluc (Δ4.5p). The cell lysates were prepared at the indicated times, and their luciferase activities were measured. (F) Stability of JEV NS4B protein in ERAD component-deficient cells. HCT116 WT cells, as well as Derlin1- and Derlin2-knockout cells infected with JEV (MOI = 1) for 48 h were treated with 50 μg/ml CHX and then collected at the indicated time points. The relative amount of JEV NS4B was quantified by Western blotting and normalized to the initial value at the zero time point.

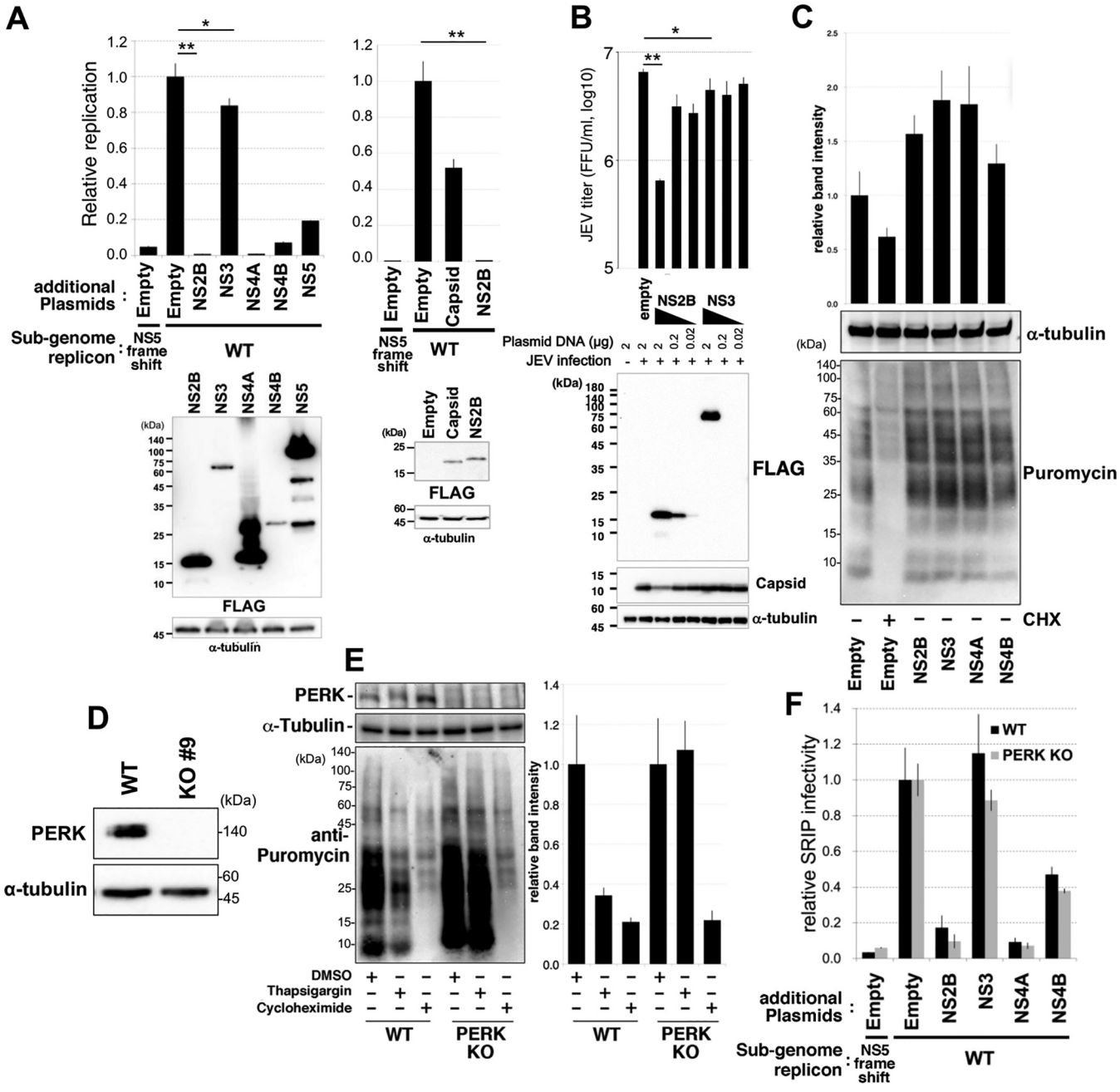

FIG 5 Overexpression of unstable NS proteins impairs viral genome replication. (A) Dominant-negative effect of some JEV proteins in terms of viral genome replication. Human 293T cells were cotransfected with pCMV(Δ4.5)-JErep-nluc (or its nonreplicable variant pCMV-Jere-nluc-fs [NS5 frameshift]) and plasmids encoding the indicated viral proteins. The cell lysates were collected at 120 h after transfection, and the luciferase activity was measured (upper graphs). Expressed viral proteins were detected by Western blotting using anti-FLAG antibody (bottom panels). **, $P < 0.05$; *, $P > 0.05$, calculated by Student's *t* test. (B) Dominant-negative effect of JEV NS2B or NS3 proteins in JEV propagation. After 6 h of JEV infection (MOI = 0.1), 1×10^5 293T cells were transfected with the indicated amounts of plasmid DNAs. After 6 h of plasmid transfection, culture medium was changed and cells were cultured for another 36 h. The JEV infectious titers in the culture supernatants were determined by a focus-forming assay (upper) and expressed NS2B, NS3, and α-tubulin were detected by Western blotting (bottom). **, $P < 0.05$; *, $P > 0.05$, calculated by Student's *t* test. (C) Effects of NS protein overexpression on host cell translation. Human 293T cells were transfected with plasmids encoding the indicated viral proteins and cultivated for 48 h. The cells were treated with 10 μg/ml puromycin 10 min before harvesting, lysed, and puromycin-incorporated proteins were detected using Western blotting with the anti-puromycin antibody (bottom). Relative puromycin signals were quantified by three independent experiments (upper). (D) The expression of endogenous PERK in PERK knockout HCT116 cells. PERK knockout HCT116 cells were lysed and endogenous PERK and α-tubulin were detected using Western blotting. (E) Deficiency of thapsigargin-mediated translational repression in PERK knockout cells. HCT116 wild-type (WT) and PERK knockout cells were treated with 1 μM thapsigargin for 1 h and the cells were incubated with 10 μg/ml puromycin during the last 10 min. The cells were also treated with 100 μg/ml CHX 15 min before puromycin labeling. The cells were lysed and puromycin-incorporated proteins were detected by Western blotting with the anti-puromycin antibody. Expression levels of PERK and α-tubulin were also tested using Western blotting (upper panel). Relative puromycin signals were quantified using the results of three independent experiments (right). (F) Dominant-negative effect of some JEV NS proteins in terms of viral particle production. HCT116 WT and PERK knockout cells were cotransfected with pCMV-JErep-nluc (or its nonreplicable variant pCMV-Jere-nluc-fs→pCMV-JErep-nluc-fs [NS5 frameshift]), pCAG-JEC (C), pCAG-JEprME (prME), and plasmids encoding the indicated viral proteins (or an empty vector [Empty]) and cultured for 72 h. The culture supernatants of the transfected cells were harvested and inoculated into Huh7 cells. After 72 h postinoculation, the luciferase activity of Huh7 cells was measured.

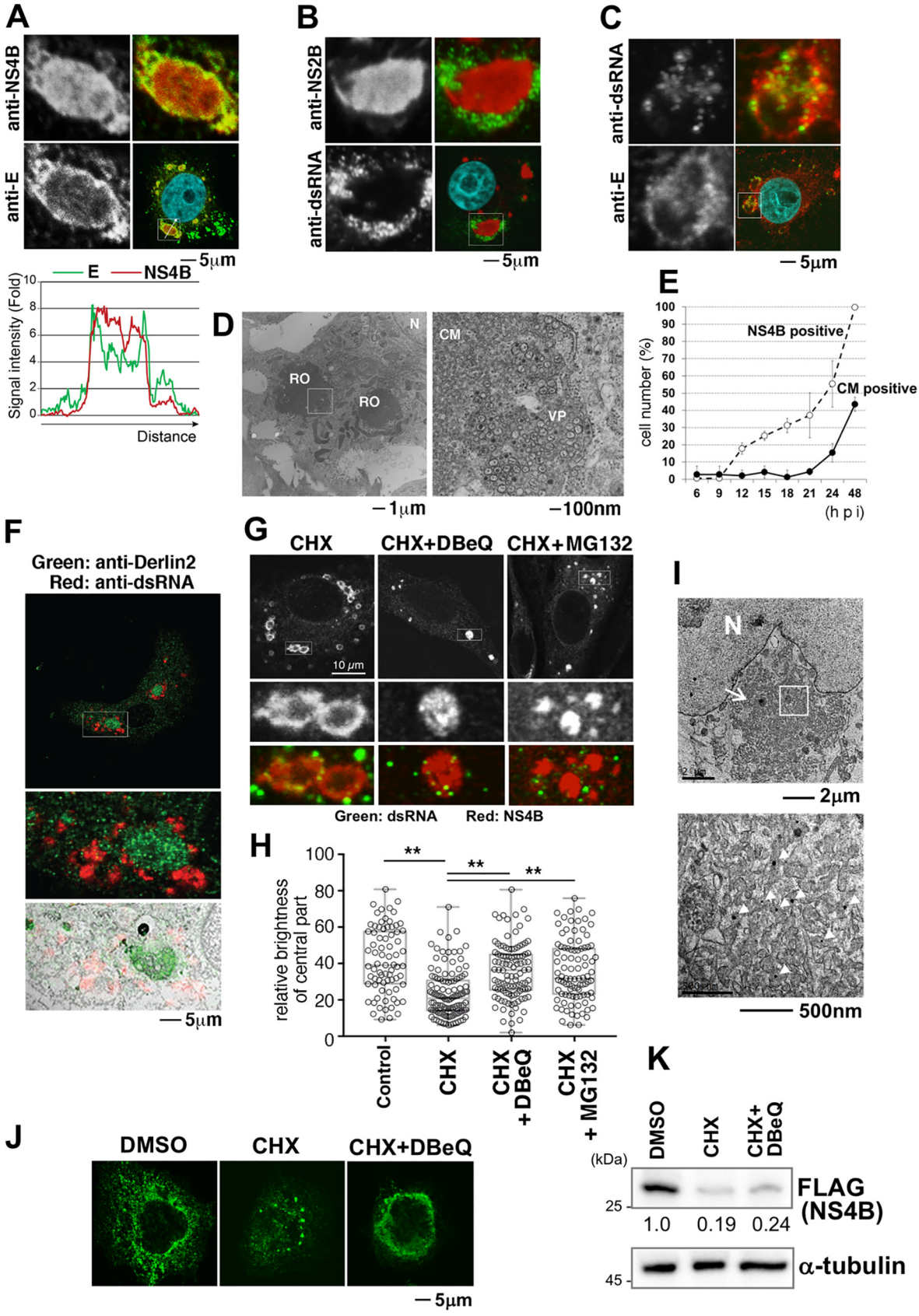

FIG 6 The role of the convoluted membrane in JEV propagation. (A to C) Different localizations of viral factors on the convoluted membrane of the virus-infected cell. Confocal microscopy images of Vero cells infected with JEV (MOI = 1) for 48 h, which had been

(Continued on next page)

ERAD pathway in the CM area of the viral replication organelle. These events are likely essential for viral propagation, as disruption of this pathway significantly impaired viral genome replication.

In most viral species, the structural and NS proteins are encoded by different mRNAs, as the requisite amounts of these proteins differ. Specifically, structural proteins form progeny virions, while NS proteins act as catalytic agents; therefore, larger quantities of structural proteins are required compared to NS proteins. Most viruses can control the amount of each viral protein at the transcriptional level; however, viruses of the *Flaviviridae* and *Picornaviridae* families do not have such properties. These viruses first synthesize a single large polypeptide containing both structural and NS proteins, after which cleavage of the polypeptide generates the individual viral proteins (2). As a result, the same amounts of structural and NS proteins are produced in these virus-infected cells. Meanwhile, the excess amount of NS proteins was harmful to viruses (Fig. 5); therefore, the viruses remove extra NS proteins that were involuntarily coproduced with the structural proteins. Our study proposes a novel model suggesting that the cellular ERAD pathway plays a central role in maintaining viral protein homeostasis. That is, *Flaviviridae* may have evolved to usurp the ERAD system to discard extra NS proteins in virus-infected cells (Fig. 7).

Previous studies on JEV revealed that this virus uses programmed −1 ribosomal frameshifting (−1 PRF) at the NS1 coding region (21). However, to date there is no direct evidence indicating that −1 PRF controls the level of structural and NS proteins. Nevertheless, it is interesting that NS1 protein is encoded at the beginning of the NS protein-coding region, and −1 PRF can produce polyproteins containing only structural proteins. Thus, we cannot exclude the possibility that this frameshift may also contribute to viral protein homeostasis.

Considering that the CM structure resembles that of the smooth ER, including the absence of ribosomes, it was previously postulated to serve as a location for the processing and storage of viral polyproteins, rather than polyprotein synthesis (4). Our results indicate that the CM may also function as the location of viral NS protein degradation. Moreover, excess NS proteins were observed to accumulate at the center of the replication organelle when the ERAD degradation system was unable to keep up with viral protein synthesis. Thus, since the appearance of the CM is dependent on specific cell types, as well as other conditions (22), perhaps it is passively generated during the

FIG 6 Legend (Continued)
fixed, and stained with anti-JEV NS4B protein and anti-JEV envelope (A), anti-JEV NS2B protein and anti-dsRNA (B), or anti-JEV envelope and anti-dsRNA (C) antibodies. Scale bar: 5 μm. The white box in the bottom right panel is enlarged in the upper right panel (dual colors) and left panels (single color). The fluorescence intensities indicated by the white arrows in A were measured and shown as red (NS4B) and green (envelope) (A, bottom graph). (D) Visualization of viral replication organelle (RO) composed of a convoluted membrane (CM) and vesicle packet (VP). A transmission electron microscopy image of Vero cells infected with JEV (MOI = 1) for 48 h. The white box shown in the left panel is enlarged in the right panel. Scale bars: 1 μm (left panel); 100 nm (right panel). (E) The emergence of CM at the late stage of viral infection. Vero cells were infected with JEV (MOI = 1), fixed at the indicated times, and stained with anti-JEV NS4B antibody. The percentage of JEV NS4B (white circles) and CM (black circles) positive cells are presented. (F) Derlin2 localized to RO. Correlative light microscopy-electron microscopy (CLEM) images of Vero cells infected with JEV (MOI = 1) for 48 h. A confocal microscopy image visualized with anti-Derlin2 (green) and anti-dsRNA (red) antibodies is presented (top and middle). The white box shown in the upper panel is enlarged in the middle panel. An ultrathin sectioned image was obtained using electron microscopy (bottom panel, merged with the fluorescent image in the middle panel). Scale bar: 5 μm (top panel). (G and H) JEV NS4B protein degradation at CM. Vero cells infected with JEV (MOI = 1) for 24 h were treated with 10 μM DBeQ and 10 μM MG132 for 2 h before treatment with 50 μg/ml CHX. After 4.5 h of CHX treatment, the cells were fixed and stained with anti-JEV NS4B and anti-dsRNA antibodies. The white boxes shown in the top panels are enlarged in the middle panels (anti-NS4B, single color) and bottom panels (red: anti-NS4B; green: anti-dsRNA) (G). Scale bar: 10 μm (top panels). (H) Scatterplots, merged with box plots, representing the ratio of the central part of the NS4B-positive structure (fluorescence intensity at the central part/total fluorescence intensity of the structure). **, $P < 0.05$, calculated using Student's *t* test. A detailed method is described in the Materials and Methods. (I) Ultrastructure of the compartment induced by JEV-NS4B expression. JEV-NS4B-GFP-expressing 293T cells were fixed and stained with anti-GFP antibody. After ultrathin sectioning, the immunostained compartment was observed by transmission electron microscopy. The white box shown in the upper panel is enlarged in the bottom panel. The arrow in the upper panel indicates the JEV-NS4B-inducing compartment. Arrowheads in the bottom panel indicate anti-GFP antibody-bounded signals. Scale bars: 2 μm (upper), 500 nm (bottom). (J and K) ERAD-mediated degradation of expressed JEV NS4B protein. (J) HeLa cells expressing JEV NS4B-FOS protein were treated with 10 μM DBeQ (right) or DMSO (middle) for 2 h before treatment with 50 μg/ml cycloheximide (CHX). After 4.5 h of CHX treatment, the cells were fixed and stained with anti-FLAG antibody. Images for negative-control cells treated with reagents are shown in the left panel. Scale bar: 5 μm. (K) Human 293T cells expressing JEV NS4B protein were treated with 10 μM DBeQ (right lane) or DMSO (middle lane) for 2 h before treatment with 50 μg/ml CHX. After 4.5 h of CHX treatment, the cells were lysed and JEV NS4B protein was detected by anti-FLAG antibody. Cell lysate from negative-control cells treated with reagents is shown in the left lane.

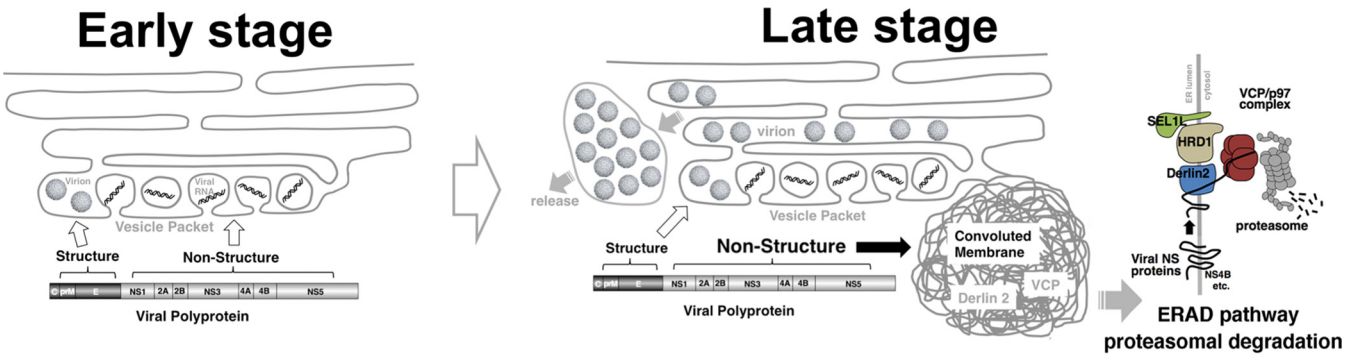

FIG 7 Model proposing the relationship between virus life cycle, cellular ERAD pathway, and convoluted membrane. Flaviviruses first synthesize a single large polypeptide containing both structural and NS proteins, which is subsequently cleaved and processed into different viral proteins. As a result, the same amount of structural and NS proteins are produced in virus-infected cells. The structural proteins form progeny virions, whereas NS proteins act as catalytic agents; therefore, the amount of structural proteins generated is higher than that of NS proteins. During the late stage of infection, viruses remove extra NS proteins that are involuntarily coproduced with the structural proteins via the cellular ERAD pathway. The convoluted membrane (CM) may function as a compartment produced passively during the later stage of infection in response to accumulated NS proteins, when the rate of ERAD degradation is slower than the rate of viral protein synthesis.

later stage of infection in response to accumulated NS proteins. Its production may be directly related to the capacity of ERAD degradation or to the speed of viral protein synthesis. In fact, structures similar to CM have also been characterized in cells infected with other viruses, including picornaviruses (23), rubiviruses (24), noroviruses (25), and coronaviruses (26). Thus, CM may represent a common structure for viruses that regulate viral protein homeostasis by ERAD.

Unfolded or misfolded proteins synthesized at the ER are known target substrates for the ERAD pathway (6). However, our results suggest that correctly folded proteins can also serve as the targets for this pathway. Although the mechanism by which viral NS proteins are recognized by ERAD remains unclear, one possibility is that specific modifications on the viral NS proteins might function as targeting signals for the ERAD pathway; alternatively, the sequestration from VP to CM might trigger the degradation.

The yeast ERAD pathway comprises three separate pathways, designated ERAD-L, ERAD-M, and ERAD-C (27). Each ERAD pathway has substrates that differ spatially, and require different components. Although exceptions exist, in general, ERAD-L primarily recognizes misfolded substrates with lesions in their luminal domains, whereas ERAD-M and ERAD-C recognize misfolded substrates with lesions in their transmembrane domains and cytoplasmic regions, respectively. The ERAD-L pathway can be further trifurcated (28, 29). One route requires Derlin2/3 and SEL1L, but not Derlin1, while the other two require Derlin1, not Derlin2/3 or SEL1L (8). In this study, we revealed that only the Derlin2/3- and SEL1L-mediated ERAD-L pathway is involved in viral protein degradation (Fig. 4C). Although the molecular mechanisms of how different ERAD pathways recognize their respective substrates remains unknown, there may be common features between viral NS proteins and cellular substrates that are degraded by the Derlin2/SEL1L-mediated ERAD pathway.

Our model does not exclude the possibility that degradation of cellular proteins by ERAD and the proteasome pathway may affect viral genome replication. Indeed, JEV infection induces degradation of HSP90 and activation of the JAK/STAT pathway to attenuate antiviral signaling (30). Meanwhile DENV suppresses the innate immune response by upregulating the expression of PDLIM2, an E3 ubiquitin ligase involved in STAT2 degradation (31). The results of the current study indicate that ERAD and proteasome inhibition inhibit degradation of these antiviral cellular proteins, while upregulating the expression of these proteins may contribute to antiviral phenotypes.

Flavivirus infection induces UPR (32, 33). In this study, we observed further upregulation of UPR following inhibition of the ERAD pathway (Fig. 3J). These results suggest that accumulation of viral proteins can trigger UPR signaling. One of the UPR sensor proteins, PERK, induces phosphorylation of eIF2-α and global translational arrest (19).

TABLE 1 Plasmids used in the study

Plasmid name	Backbone	Epitope tag	Selection	Reference
pCAG.Myc	pCAG-Myc		Amp	
pCAG.OSF	pCAG-OSF		Amp	
pCAG.JEV NS4B.FOS	pCAG-FOS	C; FLAG-One-StrEP (FOS)	Amp	
pCAG.JEV NS4B.Myc	pCAG-Myc	C, Myc	Amp	
pCAG.DENV NS4B.Myc	pCAG-Myc	C, Myc	Amp	
pCAG.OSF.NPL4_wt	pCAG-OSF	N; One-StrEP-FLAG (OSF)	Amp	
pCAG.Myc.NPL4_wt	pCAG-Myc	N, Myc	Amp	
pCAG.OSF.VCP-siR#1 (wt)	pCAG-OSF	N; One-StrEP-FLAG (OSF)	Amp	
pCAG.OSF.VCP.siR.E578Q	pCAG-OSF	N; One-StrEP-FLAG (OSF)	Amp	
pCAG.OSF.VCP.siR.E305Q/E578Q	pCAG-OSF	N; One-StrEP-FLAG (OSF)	Amp	
pCAG-NS2B-FOS	pCAG-FOS	C; FLAG-One-StrEP (FOS)	Amp	
pCAG-NS3-FOS	pCAG-FOS	C; FLAG-One-StrEP (FOS)	Amp	
pCAG-NS4A-FOS	pCAG-FOS	C; FLAG-One-StrEP (FOS)	Amp	
pCAG-NS4B-FOS	pCAG-FOS	C; FLAG-One-StrEP (FOS)	Amp	
pCAG-NS5-FOS	pCAG-FOS	C; FLAG-One-StrEP (FOS)	Amp	
pCMV-JErep-nluc			Amp	42
pCMV-JErep-nluc fs			Amp	42
pCAG-JEC			Amp	42
pCAG-JEprME			Amp	42
pCMV(Δ4.5)-JErep-nluc			Amp	
pCMV(Δ4.5)-JErep-nluc fs			Amp	
rJEV(Mie/41/2002)/pMW119			Amp	37

However, this signaling is not involved in the impairment of viral propagation, as our results show that accumulation of viral proteins impaired viral genome replication even in PERK knockout cells (Fig. 5F). UPR may promote viral genome replication by inducing chaperone expression, which guides the folding of viral and cellular proteins. Although it remains unclear how viral NS protein accumulation impairs viral genome replication, all ERAD-targeted viral proteins are anchored in the one-side leaflet of ER membranes, leading to their bending (34); therefore, the accumulation of these proteins may disrupt the proper formations of VPs that are critical for viral genome replication.

Our study reveals that VCP depletion markedly reduces viral genome replication in infected cells. Several specific small compounds that inhibit the ATPase activity of VCP similarly impair viral genome replication (Fig. 3). Recently, other specific inhibitors of VCP have been developed (35), which may represent potential antiviral drug candidates for human-pathogenic flaviviruses, such as DENV and JEV.

MATERIALS AND METHODS

Cells, viruses, and transfection. The 293A, 293T, HeLa, Huh7, BHK-21, Vero cells, and HCT116-derived knockout cell lines were cultured in Dulbecco's modified Eagle medium (DMEM; Nacalai Tesque) containing 100 units/ml penicillin, 100 μg/ml streptomycin, and 10% (vol/vol) fetal calf serum (FCS), in humidified air containing 5% CO_2 at 37°C. C6/36 cells were cultured in Schneider's insect medium (Sigma-Aldrich) at 25°C. JEV AT31 strain (kindly provided by Eiji Konishi, Osaka University) and DENV 2 NGC strain (ATCC VR-1584) were amplified in 293A and C6/36 cells, respectively. For transfection, PEI MAX (Polysciences) or Lipofectamine 3000 (Thermo Fisher Scientific) were used according to the manufacturer's instructions.

Reagents. All reagents and resources used in this study are listed in Table 1, Table 2, and Table 3. CHX (Nacalai Tesque), DBeQ (Sigma-Aldrich), Eer1 (Sigma-Aldrich), MDBN (StressMarq Biosciences), and MG132 (ECM Biosciences) were dissolved in dimethyl sulfoxide (DMSO) to prepare stock solutions.

Cycloheximide chase analysis. Cycloheximide (CHX) chase analysis was performed as described previously with slight modifications (8). In brief, 5×10^5 cells cultured in 6-well plates were infected with JEV at a multiplicity of infection (MOI) of 1 for 48 h. The cells were treated with 50 μg/ml CHX and lysed with Laemmli's sample buffer at each time point. SDS-PAGE and Western blotting were performed with antibodies for each protein. Membranes were developed using EzWestLumi plus (ATTO), and signals were detected using iBRIGHT CL1000 (Thermo Fisher Scientific). Band intensities were quantified using ImageJ/Fiji.

Purification of NS4B proteins and identification of copurified proteins by mass spectrometry. Following transient expression of Strep-tagged flaviviral NS4B in 293T cells, affinity purification was performed using Strep-Tactin Sepharose beads, and copurified proteins were identified by mass spectrometry,

TABLE 2 Antibodies used in the study

Target	Host	Clone	Source	Comment
JEV capsid	rabbit		original	Reference 43
JEV prM	rabbit		GeneTex	GTX131833
JEV E	rabbit		GeneTex	GTX125867
JEV E	mouse	6B4A-10	Merck	MAB8743
JEV NS1'	mouse	GT25111	GeneTex	GTX633961
JEV NS2B	rabbit		GeneTex	GTX125972
JEV NS3	rabbit		original	Reference 20
JEV NS4A	rabbit		GeneTex	GTX132028
JEV NS4B	rabbit		GeneTex	GTX125865
JEV NS5	rabbit		original	Immunized JEV NS5 (Pos: 691–709)
DENV NS4B	rabbit		Sigma	SAB2700180
dsRNA	mouse	J2	English & Scientific Consulting Kft.	
VCP	rabbit		Cell Signaling Technology	No. 2648
Derlin1	mouse	DERLIN1-1	Sigma	SAB4200148
Derlin2	rabbit		Sigma	D1194
FLAG	mouse	M2	Sigma	F1804
Myc	mouse	9E10	DSHB	
α-tubulin	mouse	AA4.3	DSHB	
Synoviolin (HRD1)	rabbit		Bethyl Laboratories	A302-946A
Puromycin	mouse	12D10	Merck	MABE343
PERK	rabbit		Cell Signaling Technology	3192S
NPL4	rabbit		Sigma	HPA021560
ubiquitin	mouse	FK2	MBL	D058-3
DENV capsid	rabbit		original	Immunized DENV capsid (Pos: 1–100)
GAPDH	rabbit		TREVIGEN	2275-PC-100
beta-actin	mouse		WAKO	017-24573
SEL1L	rabbit		a kind gift from Nobuko Hosokawa	Reference 44

as previously described (36). Identification of copurified proteins was carried out according to the following steps: SDS-PAGE separation, band excision, digestion with trypsin, and liquid chromatography with tandem mass spectrometry (LC-MS/MS). Tandem mass spectra were collected automatically and identified based on a nonredundant human database on NCBI.

Strep-Tactin pulldown. Twenty-four hours after 293T cells were transfected with pCAG-OSF-VCP, they were infected with JEV at an MOI of 3. The cells were lysed with lysis buffer (150 mM NaCl, 20 mM Tris-HCl [pH 7.5], and 1% Triton X-100) supplemented with complete protease inhibitor cocktail (Roche) 48 hpi. After centrifugation at 20,000 $\times$ *g* and 4°C for 10 min, the lysate was incubated with Strep-Tactin Sepharose beads (IBA GmbH) for 1 h at 4°C. The beads were then washed four times with lysis buffer supplemented with 0.1% Triton X-100 and incubated with Laemmli's sample buffer for 5 min at 95°C. The input lysate and eluate were then subjected to Western blotting.

siRNA knockdown and rescue. The siRNA knockdown and rescue experiments were performed as described previously (20). The list of siRNA target sequences is presented in Table 3.

***In vitro* transcription of the JEV RNA genome.** rJEV(Mie/41/2002)/pMW119, kindly provided by Shigeru Tajima in NIID (37), was linearized with NdeI and transcribed *in vitro* using mMESSAGE mMACHINE T7 kit (Ambion).

Focus-forming assay. Viral titers were determined using a focus-forming assay. In brief, Vero and BHK-21 monolayers cultured in 96-well plates were inoculated with serially diluted JEV and DENV, respectively, for 2 h. Next, the cells were overlaid with DMEM supplemented with 1% methylcellulose and cultured for 34 (JEV) or 58 (DENV) h. The foci of viral infection were fluoroimmunostained, as described below, using rabbit anti-JEV NS3 antibody and rabbit anti-DENV capsid antibody, respectively. Fluorescent foci of infection were counted using a fluorescence microscope, and viral infectious titers were calculated as focus-forming units per ml.

TABLE 3 siRNA target sequences

Name	Sense sequence
Control	CGUACGCGGAAUACUUCGAtt
VCP_252	GAAUAGAGUUGUUCGGAAUtt
VCP_1095	GGAGGUAGAUAUUGGAAUUtt
Npl4_878	CUGAAGUGGUCGAUGAAAUtt
Npl4_55	ACAGCAACAAAGAGAGAAAtt
HRD1_170	UGGGCAAGGUGAUGGGCAAtt
HRD1_1544	CCGCCAUGCUGCAGAUCAAtt

Virus genome replication assay using plasmid-based JEV subgenomic replicon system. We used the plasmid-based subgenomic JEV replicon, designated pCMV(Δ4.5p)-JErep-nluc, developed from a previously described plasmid called pCMV-JErep-nluc (38). In this system, an extensive region of the CMV promoter sequence was deleted, effectively attenuating its expression (39). This system allows for the minimization of background NanoLuc luciferase activity derived from plasmid-driven mRNA. cDNA of the JEV Nakayama strain containing the NanoLuc luciferase gene was inserted downstream of the attenuated CMV promoter (39). Hepatitis delta virus ribozyme (HDV-RZ) and simian virus 40 polyadenylation signal were inserted downstream of JEV cDNA. The C-prM-E coding region of JEV cDNA was replaced by NanoLuc luciferase fused with foot-and-mouth disease virus (FMDV) 2A peptide coding sequence. pCMV(Δ4.5p)-JErep-nluc was transfected into 293T cells using PEI MAX. NanoLuc luciferase activity in the cell lysate was measured according to the manufacturer's instruction (Promega).

Preparation and titration of single-round infectious particles. Preparation and titration of single-round infectious particles (SRIPs) were performed as described previously (38). In brief, cells were cotransfected with pCMV-JErep-nluc, pCAG-JEprME, and pCAG-JEC. The supernatant was harvested at 72 h posttransfection and used as SRIP supernatant. Huh7 cells were grown in a 96-well plate and inoculated with SRIP supernatant for 72 h to estimate the infectious titer of the SRIPs, and NanoLuc luciferase activity in the cell lysate was measured.

Cell viability. CellTiter-Glo luminescent cell viability assay kit (Promega) was used to evaluate cytotoxicity, as described previously (20).

Immunostaining and confocal microscopy. Cells cultured on glass coverslips were fixed with 4% paraformaldehyde in phosphate-buffered saline (PBS; Nacalai Tesque) for 15 min and subsequently permeabilized with 0.1% Triton X-100 in PBS. Cells were blocked with 10% FCS in PBS and incubated with diluted primary antibodies. Next, cells were incubated with secondary antibodies conjugated with Alexa Fluor 488 or 594 (Thermo Fisher Scientific) and nuclei were stained with Hoechst 33258 stain (Thermo Fisher Scientific). The coverslips were mounted onto slides using Fluoromount-G (SouthernBiotech). Images were acquired using a FluoView FV3000 confocal laser scanning microscope (Olympus) with a UPLAPO 60×/1.35 numerical-aperture oil immersion objective (Olympus). Image analyses were performed using ImageJ/Fiji. For staining against endogenous Derlin1 or Derlin2, cells were fixed with cold methanol for 6 min at −20°C.

Quantitative real-time PCR. Total RNA for quantitative real-time PCR (qRT-PCR) was prepared from cells using TRIzol reagent (Thermo Fisher Scientific) and converted into cDNA using the Transcriptor First Strand cDNA synthesis kit (Roche). The cDNA was amplified and quantified by real-time PCR on a PRISM 7900HT system (Applied Biosystems), with power SYBER green PCR master mix (Applied Biosystems). The following primers were used: JEV NS5-F, 5′-GCCGGGTGGGACACTAGAAT-3′; JEV NS5-R, 5′-TGGACAGCGATGTTCGTGAA-3′; GRP78-F, 5′-GAACGTCTGATTGGCGATGC-3′; GRP78-R, 5′-TCAACCACCTTGAACGGCAA-3′; CHOP-F, 5′-CCTCCTGGAAATGAAGAGGAAG-3′; CHOP-R, 5′-GTGACCTCTGCTGGTTCTGG-3′; beta-actin-F, 5′-CCAGCTCACCATGGATGATG-3′; beta-actin-R, 5′-ATGCCGGAGCCGTTGTC-3′.

Statistical analysis. All statistical analyses were performed using Microsoft Excel or GraphPad Prism (v7; GraphPad software). Two-tailed student's *t* tests were performed for unpaired or paired groups on GraphPad Prism v7 software. We also performed one-way analysis of variance followed by Dunnett's test. Data are presented as mean ± standard deviation. A P value < 0.05 was considered statistically significant. Degrees of statistical significance are indicated in the figure legends.

Correlative light and electron microscopy. CLEM (correlative light and electron microscopy) was performed as described previously with slight modifications (40). Vero cells in gridded 35-mm glass-bottom dishes (P35G-2-14-CGRD; Mat-Tek) were infected with JEV at an MOI of 1. After 6 h, the cells were washed and incubated with fresh medium for 42 h. The cells were then fixed with cold methanol at −20°C for 6 min and washed with PBS containing 4% sucrose three times for 5 min each. The cells were permeabilized with PBS containing 0.1% saponin for 30 min at 25°C. After washing with PBS, the cells were incubated in PBS containing 10% FCS and 0.005% saponin for 30 min at room temperature. As primary antibodies, rabbit anti-Derlin2 (D1194, Merck) and mouse anti-dsRNA (J2-1201, English & Scientific Consulting) were added and incubated overnight at 4°C. After washing with PBS, the cells were incubated with Alexa Fluor 488-labeled anti-rabbit and Alexa Fluor 568-labeled anti-mouse antibodies in blocking solution for 1 h at room temperature, then washed with PBS. Fluorescent images of target cells were taken at 100× magnification using a confocal laser scanning microscope. In addition, a differential interference contrast image of the same target cell was acquired to confirm its location in the dish. After imaging, cells were fixed again with 2.5% GA, 2% sucrose in 50 mM sodium cacodylate buffer (CaCo), supplemented with 50 mM KCl, 2.6 mM $MgCl_2$, and 2.6 mM $CaCl_2$ for at least 30 min at room temperature. After five washes with 50 mM CaCo, cells were incubated with 2% osmium tetroxide in 50 mM CaCo for 40 min on ice, washed three times with water, and incubated in 0.5% uranyl acetate in water overnight at 4°C. Samples were then washed three times with water, dehydrated in a graded ethanol series (from 50% to 100%) at room temperature, embedded in Epon 812 (Electron Microscopy Sciences), and polymerized for 2 days at 60°C. Ultrathin sections (70 nm) were then obtained using Leica EM UC6 (Leica Microsystems) and mounted on a grid. Sections were stained using 3% uranyl acetate in 70% methanol for 5 min and lead citrate (Reynold's) for 2 min. EM images were taken using a JEOL JEM-1400 (JEOL).

Immunoelectron microscopic analysis. Immunoelectron microscopic analysis was performed as described previously (40). Briefly, after fixation with 4% paraformaldehyde, NS4B-GFP-expressing 293T cells were permeabilized with 0.25% (wt/vol) saponin in 0.1 M PB (0.3 M sodium phosphate buffer, pH 7.4) for 30 min at room temperature, followed by treatment with blocking solution A (0.005% saponin, 10% bovine serum albumin [BSA], and 10% serum in 0.1 M PB). Primary antibody staining was performed with an anti-GFP (green fluorescent protein) antibody (1:250, B-2, Santa Cruz Biotechnology). Subsequently, cells were

washed six times with rinse solution (0.005% [wt/vol] saponin in PB), and reacted with nanogold Fab′ conjugates (NanoProbes). After washing the cells with rinse solution six times, cells were fixed again with 500 l of 1% (wt/vol) glutaraldehyde in PB. Cells were washed with 50 mM glycine, 1% (wt/vol) BSA in PB, and distilled water three times each. Next, gold signal intensification was performed with the Nanoprobes Gold Enhancement kit (Nanoprobes). Briefly, cells were incubated with gold intensification mixture at room temperature for 5 min. After washing the immunogold-labeled cells once with 1 ml of 1% (wt/vol) sodium thiosulfate, cells were washed with distilled water three times. Samples were then postfixed in 1% osmium tetroxide containing 1% potassium ferrocyanide in PB for 1 h and subsequently dehydrated in a graded ethanol series (30, 50, 70, and 90%, vol/vol; 1 ml each), followed by treatment with 100% ethanol, twice for 10 min each. Next, cells were incubated on the coverslips with 50% (vol/vol) epoxy resin in ethanol for 30 min and embedded with epoxy resin. After polymerization of samples for 2 days at 60°C, ultrathin sections were generated using an ultramicrotome equipped with a diamond knife. Sectioned cells were stained with 2% (wt/vol) uranyl acetate for 1 h, and washed three times in distilled water. Cells were then stained with lead citrate for 2 min and washed three times in distilled water. Finally, samples were observed with a Hitachi H-7600 transmission electron microscope.

Generation of knockout HCT116 cells. For generating Derlin1, Derlin2, Derlin2/Derlin3, and SEL1L knockout HCT116 cells, transcription activator-like effector nuclease (TALEN)-mediated genome editing was performed as described previously (41). CRISPR/Cas9-mediated genome editing was performed using the pX459 vector (Addgene; 62988) with the following single guide RNA (sgRNA); 5′-GGACCAAGACCGTGAAAGCA-3′, to generate PERK knockout HCT116 cells.

SUPPLEMENTAL MATERIAL

Supplemental material is available online only.

SUPPLEMENTAL FILE 1, PDF file, 0.1 MB.

ACKNOWLEDGMENTS

We thank Ryosuke Suzuki for the JEV subgenomic replicon plasmids. We also thank Sigeru Tajima for the JEV infectious clone plasmids, as well as Marina Ishimura for the PERK knockout cells.

This research was supported by JSPS KAKENHI (grant numbers 23790503, 26460555, 16H01188, and 17H06413) and a Health Labor Sciences Research Grant for Research on Emerging and Reemerging Infectious Diseases (grant number 12103320). This work was also supported by JST CREST, Japan (grant number JPMJCR17H4).

We declare no conflicts of interest.

E.M. conceived the project and designed the experiments; K.T., M.A., K.I., M.K., and A.N. conducted the experiments; T.S., T.O., and K.M. generated ERAD component knockout cells. K.T., T.O., and K.M. supervised the project; E.M., K.T., M.A., and K.I. wrote the manuscript. All authors have approved the final version of the manuscript for publication.

REFERENCES

1. Yost SA, Marcotrigiano J. 2013. Viral precursor polyproteins: keys of regulation from replication to maturation. Curr Opin Virol 3:137–142. https://doi.org/10.1016/j.coviro.2013.03.009.
2. Murray CL, Jones CT, Rice CM. 2008. Architects of assembly: roles of Flaviviridae non-structural proteins in virion morphogenesis. Nat Rev Microbiol 6:699–708. https://doi.org/10.1038/nrmicro1928.
3. Neufeldt CJ, Cortese M, Acosta EG, Bartenschlager R. 2018. Rewiring cellular networks by members of the Flaviviridae family. Nat Rev Microbiol 16:125–142. https://doi.org/10.1038/nrmicro.2017.170.
4. Welsch S, Miller S, Romero-Brey I, Merz A, Bleck CKE, Walther P, Fuller SD, Antony C, Krijnse-Locker J, Bartenschlager R. 2009. Composition and three-dimensional architecture of the dengue virus replication and assembly sites. Cell Host Microbe 5:365–375. https://doi.org/10.1016/j.chom.2009.03.007.
5. Vembar SS, Brodsky JL. 2008. One step at a time: endoplasmic reticulum-associated degradation. Nat Rev Mol Cell Biol 9:944–957. https://doi.org/10.1038/nrm2546.
6. Hwang J, Qi L. 2018. Quality control in the endoplasmic reticulum: crosstalk between ERAD and UPR pathways. Trends Biochem Sci 43:593–605. https://doi.org/10.1016/j.tibs.2018.06.005.
7. Christianson JC, Olzmann JA, Shaler TA, Sowa ME, Bennett EJ, Richter CM, Tyler RE, Greenblatt EJ, Harper JW, Kopito RR. 2011. Defining human ERAD networks through an integrative mapping strategy. Nat Cell Biol 14:93–105. https://doi.org/10.1038/ncb2383.
8. Sugimoto T, Ninagawa S, Yamano S, Ishikawa T, Okada T, Takeda S, Mori K. 2017. SEL1L-dependent substrates require Derlin2/3 and Herp1/2 for endoplasmic reticulum-associated degradation. Cell Struct Funct 42:81–94. https://doi.org/10.1247/csf.17007.
9. Ninagawa S, Okada T, Takeda S, Mori K. 2011. SEL1L is required for endoplasmic reticulum-associated degradation of misfolded luminal proteins but not transmembrane proteins in chicken DT40 cell line. Cell Struct Funct 36:187–195. https://doi.org/10.1247/csf.11018.
10. Ma H, Dang Y, Wu Y, Jia G, Anaya E, Zhang J, Abraham S, Choi J-G, Shi G, Qi L, Manjunath N, Wu H. 2015. A CRISPR-based screen identifies genes essential for West-Nile-virus-induced cell death. Cell Rep 12:673–683. https://doi.org/10.1016/j.celrep.2015.06.049.
11. Marceau CD, Puschnik AS, Majzoub K, Ooi YS, Brewer SM, Fuchs G, Swaminathan K, Mata MA, Elias JE, Sarnow P, Carette JE. 2016. Genetic dissection of Flaviviridae host factors through genome-scale CRISPR screens. Nature 535:159–163. https://doi.org/10.1038/nature18631.
12. Bruderer RM, Brasseur C, Meyer HH. 2004. The AAA ATPase p97/VCP interacts with its alternative co-factors, Ufd1-Npl4 and p47, through a common bipartite binding mechanism. J Biol Chem 279:49609–49616. https://doi.org/10.1074/jbc.M408695200.

13. Meyer H, Bug M, Bremer S. 2012. Emerging functions of the VCP/p97 AAA-ATPase in the ubiquitin system. Nat Cell Biol 14:117–123. https://doi.org/10.1038/ncb2407.
14. Song C, Wang Q, Li C-CH. 2003. ATPase activity of p97-valosin-containing protein (VCP). D2 mediates the major enzyme activity, and D1 contributes to the heat-induced activity. J Biol Chem 278:3648–3655. https://doi.org/10.1074/jbc.M208422200.
15. Chou T-F, Brown SJ, Minond D, Nordin BE, Li K, Jones AC, Chase P, Porubsky PR, Stoltz BM, Schoenen FJ, Patricelli MP, Hodder P, Rosen H, Deshaies RJ. 2011. Reversible inhibitor of p97, DBeQ, impairs both ubiquitin-dependent and autophagic protein clearance pathways. Proc Natl Acad Sci U S A 108:4834–4839. https://doi.org/10.1073/pnas.1015312108.
16. Chou T-F, Deshaies RJ. 2011. Development of p97 AAA ATPase inhibitors. Autophagy 7:1091–1092. https://doi.org/10.4161/auto.7.9.16489.
17. Wang Q, Shinkre BA, Lee J-G, Weniger MA, Liu Y, Chen W, Wiestner A, Trenkle WC, Ye Y. 2010. The ERAD inhibitor Eeyarestatin I is a bifunctional compound with a membrane-binding domain and a p97/VCP inhibitory group. PLoS One 5:e15479. https://doi.org/10.1371/journal.pone.0015479.
18. Lopez-Serra P, Marcilla M, Villanueva A, Ramos-Fernandez A, Palau A, Leal L, Wahi JE, Setien-Baranda F, Szczesna K, Moutinho C, Martinez-Cardus A, Heyn H, Sandoval J, Puertas S, Vidal A, Sanjuan X, Martinez-Balibrea E, Viñals F, Perales JC, Bramsem JB, Ørntoft TF, Andersen CL, Tabernero J, McDermott U, Boxer MB, Vander Heiden MG, Albar JP, Esteller M. 2014. A DERL3-associated defect in the degradation of SLC2A1 mediates the Warburg effect. Nat Commun 5:3608–3614. https://doi.org/10.1038/ncomms4608.
19. Harding HP, Novoa I, Zhang Y, Zeng H, Wek R, Schapira M, Ron D. 2000. Regulated translation initiation controls stress-induced gene expression in mammalian cells. Mol Cell 6:1099–1108. https://doi.org/10.1016/s1097-2765(00)00108-8.
20. Tabata K, Arimoto M, Arakawa M, Nara A, Saito K, Omori H, Arai A, Ishikawa T, Konishi E, Suzuki R, Matsuura Y, Morita E. 2016. Unique requirement for ESCRT factors in flavivirus particle formation on the endoplasmic reticulum. Cell Rep 16:2339–2347. https://doi.org/10.1016/j.celrep.2016.07.068.
21. Melian EB, Hinzman E, Nagasaki T, Firth AE, Wills NM, Nouwens AS, Blitvich BJ, Leung J, Funk A, Atkins JF, Hall R, Khromykh AA. 2010. NS1' of flaviviruses in the Japanese encephalitis virus serogroup is a product of ribosomal frameshifting and plays a role in viral neuroinvasiveness. J Virol 84:1641–1647. https://doi.org/10.1128/JVI.01979-09.
22. Junjhon J, Pennington JG, Edwards TJ, Perera R, Lanman J, Kuhn RJ. 2014. Ultrastructural characterization and three-dimensional architecture of replication sites in dengue virus-infected mosquito cells. J Virol 88:4687–4697. https://doi.org/10.1128/JVI.00118-14.
23. Gosert R, Egger D, Bienz K. 2000. A cytopathic and a cell culture adapted hepatitis A virus strain differ in cell killing but not in intracellular membrane rearrangements. Virology 266:157–169. https://doi.org/10.1006/viro.1999.0070.
24. Kujala P, Ahola T, Ehsani N, Auvinen P, Vihinen H, Kääriäinen L. 1999. Intracellular distribution of rubella virus nonstructural protein P150. J Virol 73:7805–7811. https://doi.org/10.1128/JVI.73.9.7805-7811.1999.
25. Doerflinger SY, Cortese M, Romero-Brey I, Menne Z, Tubiana T, Schenk C, White PA, Bartenschlager R, Bressanelli S, Hansman GS, Lohmann V. 2017. Membrane alterations induced by nonstructural proteins of human norovirus. PLoS Pathog 13:e1006705. https://doi.org/10.1371/journal.ppat.1006705.
26. Knoops K, Kikkert M, Worm S, Zevenhoven-Dobbe JC, van der Meer Y, Koster AJ, Mommaas AM, Snijder EJ. 2008. SARS-coronavirus replication is supported by a reticulovesicular network of modified endoplasmic reticulum. PLoS Biol 6:e226. https://doi.org/10.1371/journal.pbio.0060226.
27. Xie W, Ng DTW. 2010. ERAD substrate recognition in budding yeast. Semin Cell Dev Biol 21:533–539. https://doi.org/10.1016/j.semcdb.2010.02.007.
28. Bernasconi R, Galli C, Calanca V, Nakajima T, Molinari M. 2010. Stringent requirement for HRD1, SEL1L, and OS-9/XTP3-B for disposal of ERAD-LS substrates. J Cell Biol 188:223–235. https://doi.org/10.1083/jcb.200910042.
29. Horimoto S, Ninagawa S, Okada T, Koba H, Sugimoto T, Kamiya Y, Kato K, Takeda S, Mori K. 2013. The unfolded protein response transducer ATF6 represents a novel transmembrane-type endoplasmic reticulum-associated degradation substrate requiring both mannose trimming and SEL1L protein. J Biol Chem 288:31517–31527. https://doi.org/10.1074/jbc.M113.476010.
30. Roby JA, Esser-Nobis K, Dewey-Verstelle EC, Fairgrieve MR, Schwerk J, Lu AY, Soveg FW, Hemann EA, Hatfield LD, Keller BC, Shapiro A, Forero A, Stencel-Baerenwald JE, Savan R, Gale M. 2020. Flavivirus nonstructural protein NS5 dysregulates HSP90 to broadly inhibit JAK/STAT signaling. Cells 9:899. https://doi.org/10.3390/cells9040899.
31. Joyce MA, Berry-Wynne KM, Santos DT, Addison WR, McFarlane N, Hobman T, Tyrrell DL. 2019. HCV and flaviviruses hijack cellular mechanisms for nuclear STAT2 degradation: up-regulation of PDLIM2 suppresses the innate immune response. PLoS Pathog 15:e1007949. https://doi.org/10.1371/journal.ppat.1007949.
32. Umareddy I, Pluquet O, Wang Q-Y, Vasudevan SG, Chevet E, Gu F. 2007. Dengue virus serotype infection specifies the activation of the unfolded protein response. Virol J 4:91–10. https://doi.org/10.1186/1743-422X-4-91.
33. Medigeshi GR, Lancaster AM, Hirsch AJ, Briese T, Lipkin WI, Defilippis V, Früh K, Mason PW, Nikolich-Zugich J, Nelson JA. 2007. West Nile virus infection activates the unfolded protein response, leading to CHOP induction and apoptosis. J Virol 81:10849–10860. https://doi.org/10.1128/JVI.01151-07.
34. Romero-Brey I, Bartenschlager R. 2014. Membranous replication factories induced by plus-strand RNA viruses. Viruses 6:2826–2857. https://doi.org/10.3390/v6072826.
35. Chapman E, Maksim N, la Cruz de F, La Clair JJ. 2015. Inhibitors of the AAA+ chaperone p97. Molecules 20:3027–3049. https://doi.org/10.3390/molecules20023027.
36. Morita E, Sandrin V, Chung H-Y, Morham SG, Gygi SP, Rodesch CK, Sundquist WI. 2007. Human ESCRT and ALIX proteins interact with proteins of the midbody and function in cytokinesis. EMBO J 26:4215–4227. https://doi.org/10.1038/sj.emboj.7601850.
37. Tajima S, Nerome R, Nukui Y, Kato F, Takasaki T, Kurane I. 2010. A single mutation in the Japanese encephalitis virus E protein (S123R) increases its growth rate in mouse neuroblastoma cells and its pathogenicity in mice. Virology 396:298–304. https://doi.org/10.1016/j.virol.2009.10.035.
38. Matsuda M, Yamanaka A, Yato K, Yoshii K, Watashi K, Aizaki H, Konishi E, Takasaki T, Kato T, Muramatsu M, Wakita T, Suzuki R. 2018. High-throughput neutralization assay for multiple flaviviruses based on single-round infectious particles using dengue virus type 1 reporter replicon. Sci Rep 8:16624. https://doi.org/10.1038/s41598-018-34865-y.
39. Morita E, Arii J, Christensen D, Votteler J, Sundquist WI. 2012. Attenuated protein expression vectors for use in siRNA rescue experiments. Biotechniques 0:1–5. https://doi.org/10.2144/000113909.
40. Tabata K, Nara A, Omori H, Morita E. 2019. Immuno-localization of ESCRT proteins in virus-infected cells by fluorescence and electron microscopy. Methods Mol Biol 1998:73–92. https://doi.org/10.1007/978-1-4939-9492-2_6.
41. Ninagawa S, Okada T, Sumitomo Y, Kamiya Y, Kato K, Horimoto S, Ishikawa T, Takeda S, Sakuma T, Yamamoto T, Mori K. 2014. EDEM2 initiates mammalian glycoprotein ERAD by catalyzing the first mannose trimming step. J Cell Biol 206:347–356. https://doi.org/10.1083/jcb.201404075.
42. Suzuki R, Ishikawa T, Konishi E, Matsuda M, Watashi K, Aizaki H, Takasaki T, Wakita T. 2014. Production of single-round infectious chimeric flaviviruses with DNA-based Japanese encephalitis virus replicon. J Gen Virol 95:(Pt 1) 60–65. https://doi.org/10.1099/vir.0.058008-0.
43. Ishida K, Goto S, Ishimura M, Amanuma M, Hara Y, Suzuki R, Katoh K, Morita E. 2019. Functional correlation between subcellular localizations of Japanese encephalitis virus capsid protein and virus production. J Virol 93:e00612–19. https://doi.org/10.1128/JVI.00612-19.
44. Iida Y, Fujimori T, Okawa K, Nagata K, Wada I, Hosokawa N. 2011. SEL1L protein critically determines the stability of the HRD1-SEL1L endoplasmic reticulum-associated degradation (ERAD) complex to optimize the degradation kinetics of ERAD substrates. J Biol Chem 286:16929–16939. https://doi.org/10.1074/jbc.M110.215871.